

Error Estimates for the Approximate Component Mode Synthesis Method in the Presence of Discontinuous Parameters Across the Interface

Elena Giammatteo,
Matthias Schlottbom^[0000-0002-2527-6498]

1 Introduction

Wave propagation in heterogeneous media plays a central role in many applications, such as seismic imaging [31], the design of optical and electromagnetic devices [30], and enhanced solar cell and thin-film absorption [2, 32, 27]. Assuming time-periodic fields, the wave amplitude satisfies the heterogeneous Helmholtz equation,

$$\begin{aligned} -\operatorname{div}(a\nabla u) - \kappa^2 u &= f && \text{in } \Omega, \\ a\partial_{\mathbf{n}}u - i\omega\beta u &= g && \text{on } \partial\Omega, \end{aligned} \tag{1}$$

where i is the imaginary unit, \mathbf{n} denotes the outward unit normal vector with respect to the boundary of the domain $\Omega \subset \mathbb{R}^2$, ω is the angular frequency, and $\kappa = \omega/c$ is the wavenumber. The coefficient functions a and c model material parameters, while β is related to wave transmission through $\partial\Omega$. The functions f and g model interior sources and impedance boundary conditions, respectively.

Standard finite difference and low-order finite element methods for the numerical approximation of the Helmholtz problem at high wavenumbers suffer from large dispersion errors (pollution), necessitating much finer meshes than required for accurate interpolation of the solution [1, 16]. The efficient solution of the resulting large linear systems requires adapted methods, see, e.g., [6]. To reduce pollution, several methods have been developed, such as high-order finite difference methods [29], high-order finite element methods [4, 17], boundary element methods [3, 28], discontinuous Galerkin methods [15, 19], and multiscale methods [5, 7, 10, 20].

Elena Giammatteo
Department of Applied Mathematics, University of Twente, P.O. Box 217 NL-7500 AE Enschede,
The Netherlands, e-mail: e.giammatteo@utwente.nl

Matthias Schlottbom
Department of Applied Mathematics, University of Twente, P.O. Box 217 NL-7500 AE Enschede,
The Netherlands, e-mail: m.schlottbom@utwente.nl

Here, we consider error estimates for the approximate component mode synthesis (ACMS) method, which is a multiscale method that constructs approximations using a non-overlapping domain decomposition and local solutions of the Helmholtz equation [10]; see also [13, 14] in the context of coercive elliptic problems. If the coefficients are smooth in a neighborhood of the interface of the domain decomposition, the analyses in [10, 13] apply. In practice, however, it might be infeasible to choose the domain decomposition in that way, e.g., in layered materials or for large objects embedded in a background. As a result, the parameters may be discontinuous across the interface of the domain decomposition. We quantify the reduced convergence rates that are implied by the reduced regularity of the solution near the interface. Using the implementation of the ACMS method described in [9], we numerically verify these theoretical results. Moreover, we observe improved convergence for the error on subdomains that exclude sufficiently large neighborhoods around the corner points of the discontinuity lines of a .

The manuscript is organized as follows: Sec. 2 presents preliminaries, Sec. 3 describes the ACMS method, Sec. 4 contains error estimates and regularity results, and Sec. 5 provides numerical examples.

2 Basic assumptions and well-posedness

We use standard notation for Lebesgue and Sobolev spaces; see, e.g., [12]. Throughout the manuscript, we assume that Ω is a strictly convex polygonal domain, $f \in L^2(\Omega)$ and $g \in H^{1/2}(\partial\Omega)$. Moreover, the coefficient functions $a, c \in L^\infty(\Omega)$ are such that $a \geq a_0 > 0$ and $c \geq c_0 > 0$ for some constants $a_0, c_0 \in \mathbb{R}$, and the function $\beta \in L^\infty(\partial\Omega)$ is such that either $\beta \geq \beta_0 > 0$ or $\beta \leq \beta_0 < 0$, for a given $\beta_0 \in \mathbb{R}$. Upon multiplication by test functions and integration by parts, we obtain the standard variational formulation:

$$\text{Find } u \in H^1(\Omega) : \quad C(u, v) = G(v), \quad \text{for all } v \in H^1(\Omega), \quad (2)$$

where the sesquilinear form $C : H^1(\Omega) \times H^1(\Omega) \rightarrow \mathbb{C}$ and the antilinear functional $G : H^1(\Omega) \rightarrow \mathbb{C}$ are defined by $C(u, v) = (a\nabla u, \nabla v)_\Omega - (\kappa^2 u, v)_\Omega - \iota(\omega\beta u, v)_{\partial\Omega}$, and $G(v) = (f, v)_\Omega + (g, v)_{\partial\Omega}$. The variational formulation admits a unique solution $u \in H^1(\Omega)$ [11, Thm. 2.4]. The sesquilinear form C is bounded, $|C(u, v)| \leq C_C \|u\|_{\mathcal{B}} \|v\|_{\mathcal{B}}$, with constant $C_C = C(\Omega, a, c, \beta)$ [10], where the norm $\|u\|_{\mathcal{B}}^2 = \mathcal{B}(u, u)$ is induced by the auxiliary sesquilinear form $\mathcal{B}(u, v) = (a\nabla u, \nabla v)_\Omega + (\kappa^2 u, v)_\Omega$. Under the given assumptions, the norm $\|\cdot\|_{\mathcal{B}}$ is equivalent to the standard H^1 -norm. The solution operator for the dual problem

$$\text{Find } z \in H^1(\Omega) : \quad C(v, z) = (v, \chi) \quad \text{for all } v \in H^1(\Omega) \quad (3)$$

is denoted by $T^* : L^2(\Omega) \rightarrow H^1(\Omega)$ and maps $\chi \in L^2(\Omega)$ to $z \in H^1(\Omega)$. Both the well-posedness of (3) and the bound $\|z\|_{\mathcal{B}} \leq C_{\text{stab}} \|\chi\|_{L^2(\Omega)}$ are established in [11, Thm. 2.4], where the constant C_{stab} depends on a, c, Ω , and possibly on ω .

3 The ACMS Method

The ACMS method is based on a decomposition $\mathcal{D} = \{\Omega_j, j = 1, \dots, J\}$ of Ω into J non-overlapping subdomains with polygonal boundaries and interface $\Gamma = \bigcup_{j=1}^J \partial\Omega_j$. We denote by \mathcal{E} and \mathcal{V} the set of (relatively open) edges and vertices, respectively, and consider the case of a homogeneous interior source, $f = 0$, where the solution u to (2) is determined by its trace on Γ . For $f \neq 0$, independent local Helmholtz problems have to be solved additionally [10].

To approximate $u|_{\Gamma}$ the ACMS method employs local basis functions associated to \mathcal{V} and \mathcal{E} . The vertex basis functions φ^q are linear on each edge $e \in \mathcal{E}$ such that $\varphi^q(r) = \delta_{q,r}$ for $q, r \in \mathcal{V}$, where δ is the Kronecker delta, and the corresponding vertex space is $V_{\mathcal{V}} = \text{span}\{\varphi^q : q \in \mathcal{V}\}$. For the edge basis functions, we employ the eigenfunctions of the edge-Dirichlet-Laplace operator, but other choices are possible: for each $e \in \mathcal{E}$, find $(\tau_i^e, \lambda_i^e) \in H_0^1(e) \times \mathbb{R}, i \in \mathbb{N}$, such that

$$(\partial_e \tau_i^e, \partial_e \eta)_e = \lambda_i^e (\tau_i^e, \eta)_e, \quad \text{for all } \eta \in H_0^1(e). \tag{4}$$

Although it is clear that $\lambda_i^e = (i\pi/|e|)^2$ and $\tau_i^e(x) = \sqrt{2} \sin(\sqrt{\lambda_i^e}|x-p|), p \in \partial e$, for a line segment e , we utilize the variational characterization (4) in the implementation, because it generalizes easily to curved edges, as considered in [10]. To proceed, we define $V_{\mathcal{E}} = \text{span}\{\tau_i^e : e \in \mathcal{E}, i \in \mathbb{N}\}$ and $V_{\mathcal{E}}^{I_{\mathcal{E}}} = \text{span}\{\tau_i^e : e \in \mathcal{E}, 1 \leq i \leq I_{\mathcal{E}}^e\}$, where $I_{\mathcal{E}} \in \mathbb{N}_0^{|\mathcal{E}|}$ is a multi-index. By slight abuse of notation, when the number of modes is the same on all edges, we may write $I_{\mathcal{E}}$ instead of $I_{\mathcal{E}}^e$. The space $V_{\mathcal{V}} + V_{\mathcal{E}}$ is dense in [10]

$$H^{1/2}(\Gamma) = \{v : \Gamma \rightarrow \mathbb{C} : \forall j = 1, \dots, J, \exists u_j \in H^1(\Omega_j) \text{ s.t. } u_j|_{\partial\Omega_j} = v|_{\partial\Omega_j}\}.$$

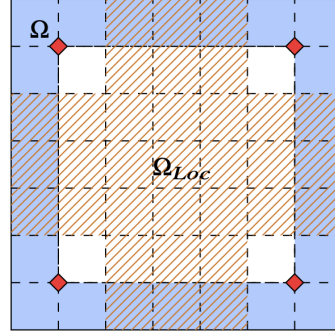
Next, we extend functions defined on Γ to Ω . For $\tau \in H^{1/2}(\partial\Omega_j)$, we let $E^j \tau \in H^1(\Omega_j)$ be such that $(E^j \tau)|_{\partial\Omega_j} = \tau$ on $\partial\Omega_j$ and

$$(a \nabla E^j \tau, \nabla \eta)_{\Omega_j} - (\kappa^2 E^j \tau, \eta)_{\Omega_j} = 0 \quad \text{for all } \eta \in H_0^1(\Omega_j).$$

Here we assume that Ω_j and ω are such that E^j is well-defined and bounded, $\|E^j \tau\|_{\mathcal{B}} \leq C_{E^j} \|\tau\|_{H^{1/2}(\partial\Omega_j)}$, see [9, 10] for a more detailed discussion. We then define $E^{\Gamma} : H^{1/2}(\Gamma) \rightarrow H^1(\Omega)$ by $(E^{\Gamma} \tau)|_{\Omega_j} = E^j(\tau|_{\partial\Omega_j})$, for $\tau \in H^{1/2}(\Gamma)$, and $j = 1, \dots, J$, and denote its norm by C_E . The ACMS space is given by $V_A(\mathcal{D}) = E^{\Gamma} V_{\mathcal{V}} + E^{\Gamma} V_{\mathcal{E}}^{I_{\mathcal{E}}}$, and the corresponding approximation reads

$$\text{Find } u_A \in V_A(\mathcal{D}) : \quad C(u_A, v_A) = G(v_A), \quad \text{for all } v_A \in V_A(\mathcal{D}). \tag{5}$$

Fig. 1 Domain $\Omega = (0, 7) \times (0, 7)$ with material parameter $a = 2$ in the white and $a = 1$ in the blue regions. The domain decomposition is shown with dashed black lines. Vertices in $\mathcal{V}_{\text{sing}}(a)$ are shown as red diamonds. In orange shading, the auxiliary domain Ω_{Loc} , used in the error computations below, which excludes the critical regions of lower regularity.



Well-posedness of (5) relies on the smallness of the adjoint approximability constant

$$\sigma^* = \sup_{\varphi \in L^2(\Omega) \setminus \{0\}} \left\{ \inf_{v_A \in V_A(\mathcal{D})} \|z - v_A\|_{\mathcal{B}} / \|\kappa\varphi\|_{L^2(\Omega)} \right\}, \quad (6)$$

where $z = E^\Gamma(T^*(\kappa^2\varphi)|_\Gamma)$, with T^* defined after (3); see [10, 11] and below.

4 Error estimates

Quantifying the approximation error of u in $V_A(\mathcal{D})$ depends on the regularity of $u|_e$. To state the corresponding regularity results, we introduce some notation and assumptions. Let $\mathcal{V}_{\text{bnd}} = \mathcal{V} \cap \partial\Omega$ denote boundary vertices. For $\epsilon > 0$ we define the tubular neighborhood of Γ by $\Gamma_\epsilon = \{x \in \Omega : \text{dist}(x, \Gamma) < \epsilon\}$. We assume that there is $\epsilon > 0$ such that the coefficient functions a and c are locally piecewise constant near Γ , i.e., $a = a_j$ and $c = c_j$ on $\Omega_j \cap \Gamma_\epsilon$. Hence, possible discontinuities in a or c do not intersect Γ . We denote by $\Gamma(a)$, resp. $\Gamma(c)$, the corresponding polygonal discontinuity curves of a , resp. c , that are contained in Γ_ϵ . We denote by $\mathcal{V}_{\text{sing}}(a)$ resp. $\mathcal{V}_{\text{sing}}(c)$ the corner points of $\Gamma(a)$ resp. $\Gamma(c)$, cf. Fig. 1. For simplicity, we assume that $\mathcal{V}_{\text{sing}}(c) \subset \mathcal{V}_{\text{sing}}(a) = \mathcal{V}_{\text{sing}}$, that $\mathcal{V}_{\text{sing}} \cap \mathcal{V}_{\text{bnd}} = \emptyset$, and that an edge $e \in \mathcal{E}$ does not connect a $p \in \mathcal{V}_{\text{bnd}}$ with a $q \in \mathcal{V}_{\text{sing}}$.

In view of [22, Lem. 1], the solution u can be decomposed into an H^2 -regular component and a singular component in a neighborhood of $p \in \mathcal{V}_{\text{sing}}$; see also [24, 25]. The regularity of the singular component depends on the values of a near p and the angles between edges $e \in \mathcal{E}$ for which $p \in \partial e$. We denote by $\alpha_{\text{sing}} \in (0, 1)$ the corresponding critical exponent. If a assumes at most two different values close to p , then $\alpha_{\text{sing}} > 1/2$. We have the following statement.

Lemma 1 *Let $e \in \mathcal{E}$ and let $\Omega_j \in \mathcal{D}$ be such that $e \subset \partial\Omega_j$. The following statements hold for the solution u to (2) with $f = 0$ and smooth g .*

- (i) *If $\partial e \cap (\mathcal{V}_{\text{sing}} \cup \mathcal{V}_{\text{bnd}}) = \emptyset$, then $u \in H^{5/2}(e)$.*

- (ii) If $\partial e \cap \mathcal{V}_{\text{sing}} \neq \emptyset$, then for all $s < \alpha_{\text{sing}} + 1/2$, $u \in H^s(e)$.
- (iii) If $\partial e \cap \mathcal{V}_{\text{bnd}} \neq \emptyset$, then $u \in H^s(e)$ for all $3/2 \leq s < 5/2$.

Proof. (i) follows from [21, Thm. 4.20]. (ii) follows from [24, Thm. 4.2]; see also [22, Cor. 2]. (iii) follows from [12, Cor. 4.4.3.8], [23, Thm. 5.1] and [12, Lem. 5.1.3.3]. \square

Corresponding regularity results for the solution of the dual problem are stated next. The main difference lies in the fact that the boundary data vanish, while the interior source term generally belongs to $L^2(\Omega)$. Consequently, the dual solution is, at best, $H^2(\Omega_j \cap \Gamma_\epsilon)$.

Lemma 2 *Let $e \in \mathcal{E}$ and let $\Omega_j \in \mathcal{D}$ such that $e \subset \partial\Omega_j$. The following statements hold for the solution $z = T^*\chi$ to the adjoint problem (3) with $\chi \in L^2(\Omega)$.*

- (i) If $\partial e \cap \mathcal{V}_{\text{sing}} = \emptyset$, then $z \in H^{3/2}(e)$ and there exists $C > 0$ such that $\|z\|_{H^{3/2}(e)} \leq C\|\chi\|_{L^2(\Omega)}$.
- (ii) If $\partial e \cap \mathcal{V}_{\text{sing}} \neq \emptyset$, then for all $s < \alpha_{\text{sing}} + 1/2$, $z \in H^s(e)$ and there exists $C > 0$ such that $\|z\|_{H^s(e)} \leq C\|\chi\|_{L^2(\Omega)}$.

Given the regularity of $u|_e$, $e \in \mathcal{E}$, estimates for $\|u - u_A\|_{H^1(\Omega)}$ can be obtained by bounding $\inf_{v \in \mathcal{V}_V + \mathcal{V}_E} \|u - v\|_{H^{1/2}(e)}$ for each $e \in \mathcal{E}$ in terms of powers of $\lambda_{I_e}^e$ [8, 10]. Also $L^2(\Omega)$ -norm error bounds follow using a duality argument [8, 10]. Below, we state a global version of such bounds, for which we introduce $\lambda^\Gamma = \min_{e \in \mathcal{E}} \lambda_{I_e}^e$. In view of Lem. 1, there are $s_e \in (1/2, 5/2)$, $e \in \mathcal{E}$, such that $u|_e \in H^{s_e}(e)$. We denote $s^* = \min_{e \in \mathcal{E}} s_e$ the smallest regularity index for the edges. Similarly, using Lem. 2, we denote $\delta_e = \min(s_e, 3/2)$, for which the solution of the dual problem satisfies $z|_e \in H^{\delta_e}(e)$, and $\delta^* = \min(s^*, 3/2)$.

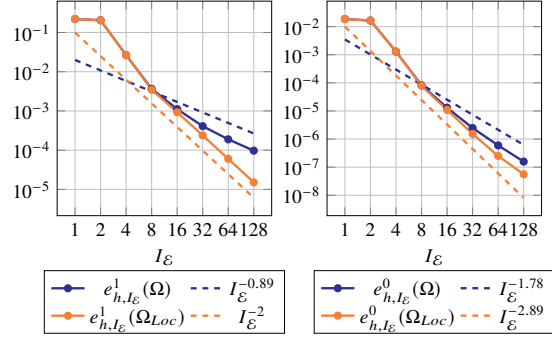
Theorem 1 *Let g be smooth. There is a constant $C = C(s^*, C_{\text{stab}}, \|\kappa\|_\infty^2, \mathcal{D}, C_E)$ such that $\sigma^* \leq C(\lambda^\Gamma)^{(1-2\delta^*)/4}$. Moreover, if $C_C\sigma^* \leq 1/2$, then there exists a unique $u_A \in V_A(\mathcal{D})$ such that (5) holds and such that*

$$\|u - u_A\|_{H^1(\Omega)} + (\lambda^\Gamma)^{\frac{2\delta^*-1}{4}} \|u - u_A\|_{L^2(\Omega)} \leq C(\lambda^\Gamma)^{-\frac{2s^*-1}{4}} \sum_{e \in \mathcal{E}} \|u\|_{H^{s_e}(e)}.$$

5 Numerical results

We verify numerically the error estimates of Thm. 1. Since the exact solution u is unknown, we replace it by a reference solution, $u^{h,10}$, computed with the open-source software package NGSolve [26] on a quasi-uniform triangulation of the domain $\Omega = (0, 7) \times (0, 7)$ with mesh size $h \approx 0.005$ and piecewise polynomials of degree 10. Here, we set the parameter $\beta = -1$, the wavenumber $\kappa = 1$, and the source terms $f = 0$ and $g(\mathbf{x}) = e^{-\iota\kappa\mathbf{x}} e^{-100|\mathbf{x}-\mathbf{x}_L|^2}$ with $\mathbf{x}_L = (0, 3.5)$. Moreover, we let $a = 2$ in $(1, 6) \times (1, 6)$ and $a = 1$ elsewhere; see Fig. 1. We choose a domain decomposition made of unit squares, illustrated with the black dashed lines

Fig. 2 Left: Relative H^1 -errors $e_{h,I_\mathcal{E}}^1(\Omega)$ (blue, solid) and $e_{h,I_\mathcal{E}}^1(\Omega_{Loc})$ (orange, solid) together with the theoretical rates (dashed) for different $I_\mathcal{E} = 2^l$, for $l = 0 \dots, 7$. Right: The same as left but for the L^2 -error.



in Fig. 1, with $J = 49$ subdomains, $|\mathcal{E}| = 112$ edges, and $|\mathcal{V}| = 64$ vertices. The numerical ACMS approximation, denoted by $u_A^{h,6}$, is computed with the NGSolve-based implementation described in [18], using the same triangulation as used in the computation of $u^{h,10}$ but with local polynomial degree 6 and an equal number of modes $I_\mathcal{E}$ on each edge. We consider the relative errors

$$e_{h,I_\mathcal{E}}^1(\Omega) = \|u^{h,10} - u_A^{h,6}\|_{H^1(\Omega)} / \|u^{h,10}\|_{H^1(\Omega)}, \tag{7}$$

$$e_{h,I_\mathcal{E}}^0(\Omega) = \|u^{h,10} - u_A^{h,6}\|_{L^2(\Omega)} / \|u^{h,10}\|_{L^2(\Omega)}, \tag{8}$$

with corresponding notation for domains other than Ω . We can compute the regularity index α_{sing} for the four critical vertices $\mathcal{V}_{\text{sing}} = \{(1, 1), (6, 1), (6, 6), (1, 6)\}$, see Fig. 1, by solving a small eigenvalue problem [22], which gives $\alpha_{\text{sing}}^* \approx 0.893$ for the considered test case. Since $\lambda^\Gamma \sim I_\mathcal{E}^2$, we thus expect a convergence rate in the H^1 -norm slightly worse than $\mathcal{O}(I_\mathcal{E}^{-\alpha_{\text{sing}}^*})$ by Thm. 1, i.e., an approximate rate of $\mathcal{O}(I_\mathcal{E}^{-0.89})$. Similarly, we expect that the adjoint approximability constant decays like $\mathcal{O}(I_\mathcal{E}^{-0.89})$, and that the L^2 -norm of the error behaves like $\mathcal{O}(I_\mathcal{E}^{-1.78})$. In Fig. 2, we plot $e_{h,I_\mathcal{E}}^1(\Omega)$ (left) and $e_{h,I_\mathcal{E}}^0(\Omega)$ (right) for different values of $I_\mathcal{E}$, together with the expected rates $\mathcal{O}(I_\mathcal{E}^{-0.89})$ and $\mathcal{O}(I_\mathcal{E}^{-1.78})$, respectively. We may conclude that the errors asymptotically achieve the theoretical rates.

If the solution was smooth on Γ_ϵ for some $\epsilon > 0$, we would expect the rates $\mathcal{O}(I_\mathcal{E}^{-2})$ and $\mathcal{O}(I_\mathcal{E}^{-3})$ in the H^1 -norm and in the L^2 -norm, respectively, cf. [10]. Since the solution is sufficiently regular on edges that do not connect to critical vertices, we also investigate the error on subdomains that do not include the critical points and the corresponding edges. To do so, we consider the domain Ω_{Loc} that is defined by removing (the closure of) all subdomains around the points in $\mathcal{V}_{\text{sing}}$; see also Fig. 1. The corresponding errors $e_{h,I_\mathcal{E}}^1(\Omega_{Loc})$ and $e_{h,I_\mathcal{E}}^0(\Omega_{Loc})$ are shown in Fig. 2, and we observe that we recover the full rate of convergence for the H^1 -error on Ω_{Loc} . The observed rate of approximately 2.89 for the L^2 -error can be explained by the fact that the L^2 -error is upper bounded by the product of the (global) adjoint approximability constant and the (localized) H^1 -error.

6 Conclusions

We extended the ACMS error analysis to cases with discontinuous parameters across interfaces and derived quantitative error bounds, verified by numerical examples. Since the solution's normal derivative is generally discontinuous across interfaces, its trace on non-aligned edges is non-smooth, causing slow convergence of the current edge modes. A possible remedy is to use piecewise-defined functions that resolve the intersection of the interface and edge. Further work includes extending the formulation and analysis to three-dimensional problems, where suitable regularity results may be exploited (cf. [24, 25]). The constant in Theorem 1 depends on the wavenumber κ . A numerical study, [9], suggests that C scales linearly with κ for the problems considered. Hence, the number of modes should (locally) increase with κ , depending on δ^* , or alternatively, the domain decomposition should be refined near critical vertices in $\mathcal{V}_{\text{sing}}$.

Acknowledgements The research of EG was supported by the Dutch Research council (NWO) via grant OCENW.GROOT.2019.071.

References

1. Babuška, I.M., Sauter, S.A.: Is the pollution effect of the FEM avoidable for the Helmholtz equation considering high wave numbers? *SIAM J. Numer. Anal.* **34**(6), 2392–2423 (1997)
2. Bermel, P., Luo, C., Zeng, L., Kimerling, L.C., Joannopoulos, J.D.: Improving thin-film crystalline silicon solar cell efficiencies with Photonic crystals. *Opt. Express* **15**(25), 16986 (2007)
3. Bruno, O.P., Garza, E., Perez-Arancibia, C.: Windowed Green function method for nonuniform open-waveguide problems. *IEEE Trans. Antennas Propag.* **65**(9), 4684–4692 (2017)
4. Chaumont-Frelet, T., Nicaise, S.: Wavenumber-explicit convergence analysis for finite element discretizations of general wave propagation problems. *IMA J. Numer. Anal.* **40**(2), 1503–1543 (2020)
5. Chen, Y., Hou, T.Y., Wang, Y.: Exponentially convergent multiscale method for 2D high frequency heterogeneous Helmholtz equations. *Multiscale Model. Simul.* **21**(3), 849–883 (2023)
6. Engquist, B., Ying, L.: Sweeping preconditioner for the Helmholtz equation: Hierarchical matrix representation. *Commun. Pure Appl. Math.* **64**(5) (2011)
7. Freese, P., Hauck, M., Peterseim, D.: Super-localized orthogonal decomposition for high-frequency Helmholtz problems. *SIAM J. Sci. Comput.* **46**(4), A2377–A2397 (2024)
8. Giammatteo, E.: On the approximate component mode synthesis method for the approximation of the Helmholtz equation. Ph.D. thesis, University of Twente (2025)
9. Giammatteo, E., Heinlein, A., Lederer, P.L., Schlottbom, M.: High-order discretized ACMS method for the simulation of finite-size two-dimensional Photonic crystals. *Comput. Math. Appl.* **196**, 376–394 (2025)
10. Giammatteo, E., Heinlein, A., Schlottbom, M.: An extension of the approximate component mode synthesis method to the heterogeneous Helmholtz equation. *IMA J. Numer. Anal.* (2024)
11. Graham, I.G., Sauter, S.A.: Stability and finite element error analysis for the Helmholtz equation with variable coefficients. *Math. Comput.* **89**(321), 105–138 (2019)
12. Grisvard, P.: *Elliptic Problems in Nonsmooth Domains*. SIAM (2011)
13. Hetmaniuk, U., Klawonn, A.: Error estimates for a two-dimensional special finite element method based on component mode synthesis. *ETNA* **41**, 109–132 (2014)

14. Hetmaniuk, U.L., Lehoucq, R.B.: A special finite element method based on component mode synthesis. *ESAIM Math. Model. Numer. Anal.* **44**(3), 401–420 (2010)
15. Hiptmair, R., Moiola, A., Perugia, I.: A survey of Trefftz methods for the Helmholtz equation. In: *Building Bridges: Connections and Challenges in Modern Approaches to Numerical Partial Differential Equations*, pp. 237–279. Springer (2016)
16. Ihlenburg, F., Babuška, I.: Finite element solution of the Helmholtz equation with high wave number. part I: The h-version of the FEM. *Comput. Math. Appl.* **30**(9), 9–37 (1995)
17. Lafontaine, D., Spence, E.A., Wunsch, J.: Wavenumber-explicit convergence of the hp-FEM for the full-space heterogeneous Helmholtz equation with smooth coefficients. *Comput. Math. Appl.* **113**, 59–69 (2022)
18. Lederer, P.L., Giammatteo, E.: ACMS: Release v1.0 (2024). DOI 10.5281/zenodo.13898693
19. Lehrenfeld, C., Stocker, P.: Embedded Trefftz discontinuous Galerkin methods. *Int. J. Numer. Methods Eng.* **124**(17), 3637–3661 (2023)
20. Ma, C., Alber, C., Scheichl, R.: Wavenumber-explicit convergence of a multiscale generalized finite element method for heterogeneous Helmholtz problems. *SIAM J. Numer. Anal.* **61**(3), 1546–1584 (2023)
21. McLean, W.C.H.: *Strongly Elliptic Systems and Boundary Integral Equations*. Cambridge Univ. Press (2000)
22. Mercier, D.: Minimal regularity of the solutions of some transmission problems. *Math. Methods Appl. Sci.* **26**(4), 321–348 (2003)
23. Mghazli, Z.: Regularity of an elliptic problem with mixed Dirichlet–Robin boundary conditions in a polygonal domain. *Calcolo* **29**(3–4), 241–267 (1992)
24. Nicaise, S., Sändig, A.: General interface problems—I. *Math. Methods Appl. Sci.* **17**(6), 395–429 (1994)
25. Nicaise, S., Sändig, A.: General interface problems—II. *Math. Methods Appl. Sci.* **17**(6), 431–450 (1994)
26. Schoeberl, J., NGSolve Contributors: NGSolve/ngsolve: v6.2.2404 (2024)
27. Sharma, D., Hasan, S.B., Saive, R., van der Vegt, J.J.W., Vos, W.L.: Enhanced absorption in thin and ultrathin silicon films by 3d Photonic band gap back reflectors. *Opt. Express* **29**(25), 41023 (2021)
28. Strauszer-Caussade, T., Faria, L.M., Fernandez-Lado, A., Pérez-Arancibia, C.: Windowed Green function method for wave scattering by periodic arrays of 2D obstacles. *Stud. Appl. Math.* **150**(1), 277–315 (2023)
29. Tong, C., Fang, X., Zhao, M.: Fast high-order algorithm for three-dimensional Helmholtz equation involving impedance boundary condition with large wave numbers. *Am. J. Comput. Math.* **13**(2), 211–229 (2023)
30. Wang, J., Qi, M.: Design of a compact mode and polarization converter in three-dimensional Photonic crystals. *Opt. Express* **20**(18), 20356 (2012)
31. Wang, S., de Hoop, M.V., Xia, J.: On 3D modeling of seismic wave propagation via a structured parallel multifrontal direct Helmholtz solver. *Geophys. Prospect.* **59**(5), 857–873 (2011)
32. Zhou, D., Biswas, R.: Photonic crystal enhanced light-trapping in thin film solar cells. *J. Appl. Phys.* **103**(9) (2008)